


# Strange metal behavior from incoherent carriers scattered by local moments

Sergio Ciuchi<sup>1</sup> and Simone Fratini<sup>2</sup>

<sup>1</sup>*Dipartimento di Scienze Fisiche e Chimiche, Università dell'Aquila, Coppito-L'Aquila, Italy  
and Istituto dei Sistemi Complessi, CNR, 00185 Roma, Italy*

<sup>2</sup>*Université Grenoble Alpes, CNRS, Grenoble INP, Institut Néel, 38000 Grenoble, France*

 (Received 11 July 2023; revised 7 December 2023; accepted 11 December 2023; published 27 December 2023)

We study metallic transport in an effective model that describes the coupling of electrons to fluctuating magnetic moments with full SU(2) symmetry, exhibiting characteristic behavior of metals at the approach of the Mott transition. We show that scattering by fluctuating local moments causes a fully incoherent regime of electron transport with  $T$ -linear resistivity. This strange metal regime is characterized by almost universal, nearly Planckian slope and a finite zero-temperature intercept, that we can associate respectively with the amplitude fluctuations and with the random orientations of local magnetic moments. Our results indicate a route for understanding the microscopic origin of strange metal behavior that is unrelated to quantum criticality and does not rely on the existence of quasiparticles.

DOI: [10.1103/PhysRevB.108.235173](https://doi.org/10.1103/PhysRevB.108.235173)

## I. INTRODUCTION

One of the open theoretical challenges in quantum materials is the explanation of strange metal behavior: in many complex metals the resistivity increases approximately linearly with temperature over an extended temperature range, as  $\rho(T) \simeq \rho_0 + BT$  instead of the expected quadratic behavior, therefore contradicting the very foundations of Fermi liquid theory. The slope of  $\rho(T)$  has been the subject of thorough investigation, and is now often interpreted as an indication of a fundamental “Planckian” bound for inelastic scattering [1–5]. The residual term  $\rho_0$  has received less attention. Both numerical studies [6,7] and experiments [8] indicate that the latter amounts to a  $T$ -independent shift of the resistivity curves upon tuning the interaction strength, which is strongly reminiscent of the effects of elastic disorder scattering [9]. The precise origin of such intrinsically generated disorder is still unclear [10].

In order to pinpoint the microscopic origin of the reported strange metal phenomenology, we introduce here a microscopic model that considers the coupling of electrons to fluctuating local moments while setting aside all the more complex many-body effects contained in the Hubbard model. This reductionist approach captures the key aspects of the previously calculated resistivity of correlated metals at the approach of the Mott transition in the high-temperature regime, revealing the essential microscopic transport processes at play.

In qualitative agreement with available numerical treatments of correlated electron transport in the framework of the Hubbard model [11–16] we find a resistivity that varies linearly with temperature with a slope that is qualitatively compatible with Planckian bounds.

Our formulation of the problem demonstrates that the ubiquitous  $T$ -linear behavior as well as the finite intercept both originate from the scattering by local magnetic fluctuations, in a regime where the current is not carried by individual quasiparticles. The theory draws a direct connection between

the anomalous electronic transport properties and the SU(2) nature of the scatterers, through their ability to fluctuate both in size and in orientation. Finally, the addition of even modest disorder scattering in the scalar charge sector can stabilize linear resistivity down to the lowest temperatures, as is observed in a variety of correlated metals.

## II. MODEL AND METHOD

We consider a model of electrons moving on a lattice and that are coupled with local magnetic fluctuations. These arise in Mott systems when electronic correlations constrain the electrons to single occupancy on atomic sites. In full generality, our model can also mimic other types of local fluctuations (e.g., of stripe order) scattering the electronic carriers [17]. We consider the action  $S = S_0 + S_{\text{int}} + S_b$  with

$$S_0 = \int d\tau \sum_{i,j,\sigma} \bar{c}_{i,\sigma}(\tau) [\delta_{i,j}(\partial_\tau - \mu) - t_{ij}] c_{j,\sigma}(\tau'), \quad (1)$$

$$S_{\text{int}} = \int d\tau \sum_{\sigma,\rho} \sum_{v,i} g_v \bar{c}_{i,\sigma}(\tau) \sigma_{\sigma,\rho}^v c_{i,\rho}(\tau) X_i^v, \quad (2)$$

$$S_b = \frac{\beta}{2} \sum_{v,i} k_v (X_i^v)^2. \quad (3)$$

$S_0$  describes tight binding electrons moving on a lattice with intersite transfer integrals  $t_{ij}$  defined as Grassman variables  $c_{i\sigma}$ ,  $\bar{c}_{i\sigma}$  at lattice site  $i$  and with spin  $\sigma$ . Throughout this work we set the particle density to half filling.

The interaction term,  $S_{\text{int}}$ , describes the local coupling of the electrons with classical variables of bosonic origin,  $X_i^v$ , governed by the harmonic term  $S_b$ . The vector part ( $v = 1, 2, 3$ ) represents the interaction with fluctuating local moments. Formally, a SU(2) symmetric spin-boson interaction can be rigorously derived by linearizing the Hubbard model via a Hubbard-Stratonovich transformation and then taking the high-temperature limit, yielding  $g_v = 1$  and  $k_v = 3/U$  [18,19]. The scalar part of  $S_{\text{int}}$  (index  $v = 0$ ) nominally

represents a local coupling with the charge, and has been thoroughly studied elsewhere [20]. In a broader sense, the latter can also serve as a proxy for retarded, longer-ranged Coulomb interactions between electrons. All along this work we consider an isotropic spin coupling  $g_{1,2,3} = g_s$ , preserving SU(2) symmetry; in this case the relevant quantity that couples to the electron spin is the energy fluctuation associated with the radial bosonic variable  $v = g_s r = g_s \sqrt{\sum_{\nu=1}^3 (X^\nu)^2}$ , with  $\lambda_s = g_s^2/2k_s D$  the corresponding dimensionless coupling strength, where  $D$  is the half bandwidth for the no-interacting model  $S_0$  (see [21] for a real-space implementation of the theory, and [22] for a related approach for Ising spins). Connecting to the original Hubbard model via the Hubbard-Stratonovich derivation yields  $(U/D) = 6\lambda_s$  [18].

Because we are interested in high-temperature transport, we have deliberately omitted the boson dynamics in Eq. (3) [18]. This approximation, that is consistently validated by our results shown next, is appropriate to the problem at hand as it applies in regimes where the relevant bosonic (spin and/or charge) fluctuations are slow, a situation that is favored by the presence of strong many-body correlations. Crucially to the remainder of this work, this setup explicitly shows how the bosons can act as a thermalized disordered environment for the electrons whenever the temperature is larger than the relevant bosonic energy scale. To derive all quantities of interest from the action Eqs. (1)–(3) we use single-site dynamical mean field theory (DMFT) [23] in a nonmagnetically ordered phase, assuming a semicircular density of states (DOS) for the noninteracting electrons (see Appendix A). For static bosons the impurity model can be solved exactly. The local Green's function  $G$  can then be calculated as a statistical average over the thermal distribution  $\mathcal{P}(v)$  of local boson energy fluctuations. The corresponding electron self-energy  $\Sigma$  is obtained via the usual self-consistency condition,  $\Sigma(\omega) = \omega - \frac{D^2}{4} G(\omega) - G^{-1}(\omega)$  for the chosen semicircular DOS. The electrical conductivity is calculated via the Kubo formula:

$$\sigma(T) = 2\bar{\sigma}\pi \int d\epsilon \Phi(\epsilon) \int d\omega A^2(\epsilon, \omega) \left( -\frac{df}{d\omega} \right), \quad (4)$$

where  $A(\epsilon, \omega) = -\text{Im}[\omega - \epsilon - \Sigma(\omega)]^{-1}/\pi$  is the spectral function,  $f$  is the Fermi function and  $\Phi(\epsilon)$  is the transport function of the lattice model, given by the DOS of the squared velocity along a given direction. This treatment explicitly ignores vertex corrections; these are known to moderately suppress the resistivity without however altering the form of its temperature dependence, that is our main interest here. [7]. Conductivity units are set by  $\bar{\sigma} = e^2 a^2/\hbar\Omega$  with  $a$  the lattice parameter in the relevant direction and  $\Omega$  the unit cell volume (see Appendix B).

### III. CORRELATED BEHAVIOR AND MOTT TRANSITION

Figure 1 shows resistivity vs temperature curves for increasing values of the coupling parameter  $\lambda_s$ . At all temperatures higher than the Fermi liquid temperature, our results reproduce the essential features observed at the approach and across the Mott transition in the Hubbard model [6,7]. Incidentally, the metal-insulator transition (MIT) is found here at  $\lambda_s^c = 0.36$ , corresponding to  $(U/D)_c = 2.2$ , in good

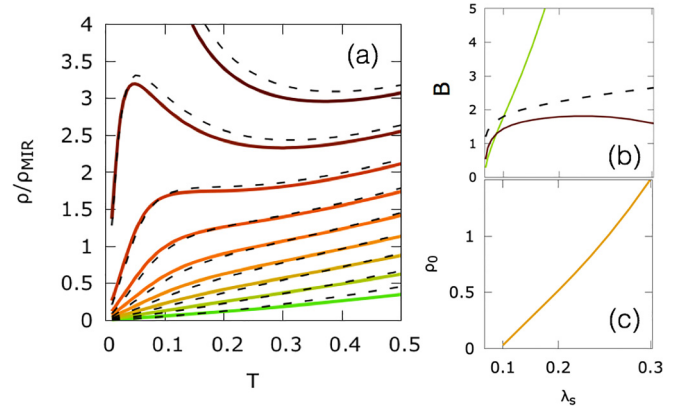


FIG. 1. (a) Temperature dependent resistivity calculated for equally spaced  $\lambda_s = 0.04 \rightarrow 0.36$ , in units of  $\rho_{\text{MIR}}$ . Dashed lines are the results of the incoherent approximation (see text and Appendix C). (b) Temperature coefficient of the resistivity  $B$  at low ( $T = 0.05$ , green) and high temperature ( $T = 0.5$ , brown) as a function of  $\lambda_s$  in quadratic scale, together with the prediction of the incoherent approximation (dashed). (c) The zero temperature intercept  $\rho_0$  (residual resistivity) extrapolated from high temperatures.

agreement with the single-site continuous-time quantum Monte Carlo (CTQMC) result in the half-filled Hubbard model,  $(U/D)_c = 2.3$  [24].

We find two fundamentally different  $T$ -linear resistivity regimes. At low temperatures, only states near the Fermi energy contribute to transport. In this “resilient quasiparticle” regime [25], one can tentatively apply the weak-scattering, low- $T$  limit of Eq. (4), namely  $\rho/\rho_{\text{MIR}} = \Gamma/2D$  [with the resistivity at the Mott-Ioffe-Regel limit given by  $\rho_{\text{MIR}} = (3\pi/2)/\bar{\sigma}$ ; see Appendix B]. Observing that the coupling to thermal bosons yields  $\Gamma \propto \lambda_s T$  [26] leads to a resistivity that is trivially linear in temperature, with a large variability in slopes upon varying  $\lambda_s$ , and a common intercept  $\rho_0 = 0$ . This indeed agrees with what is seen in Fig. 1(a) at low  $T$ . The slopes shown in Fig. 1(b) (green), however, markedly contradict this weak-scattering prediction, as they increase with  $\lambda_s^2$  [27] instead of  $\lambda_s$ .

For sufficiently large  $\lambda_s$  still within the metallic phase the system enters a second linear regime upon increasing the temperature: here the slope  $B$  is similar for all curves, while the  $\rho_0$  intercept is nonzero and is strongly parameter dependent [Figs. 1(a) and (c)]. The slope itself is of order of unity when expressed in the natural units of the model, i.e.,  $B = d(\rho/\rho_{\text{MIR}})/d(T/D) \simeq 1.5$ –2 [Fig. 1(b) and map Fig. 2(f)], in quantitative agreement with numerical studies on the Hubbard model [11–16] as well as with recent transport measurements of correlated organic metals as a function of pressure [8]. If we were to interpret this result within the weak-scattering/low-temperature Drude picture, as is customarily done in experiments [2–4,28], we would obtain  $d\Gamma/dk_B T = 2B$ , yielding  $d\Gamma/dT$  of order of a few  $k_B$ , with a clear Planckian flavor. The overall behavior found in this high-temperature regime is very reminiscent of the phenomenology observed in strange metals.

*Emergence of local moments.* We now show that the strange metal behavior found at high  $T$  is a direct consequence

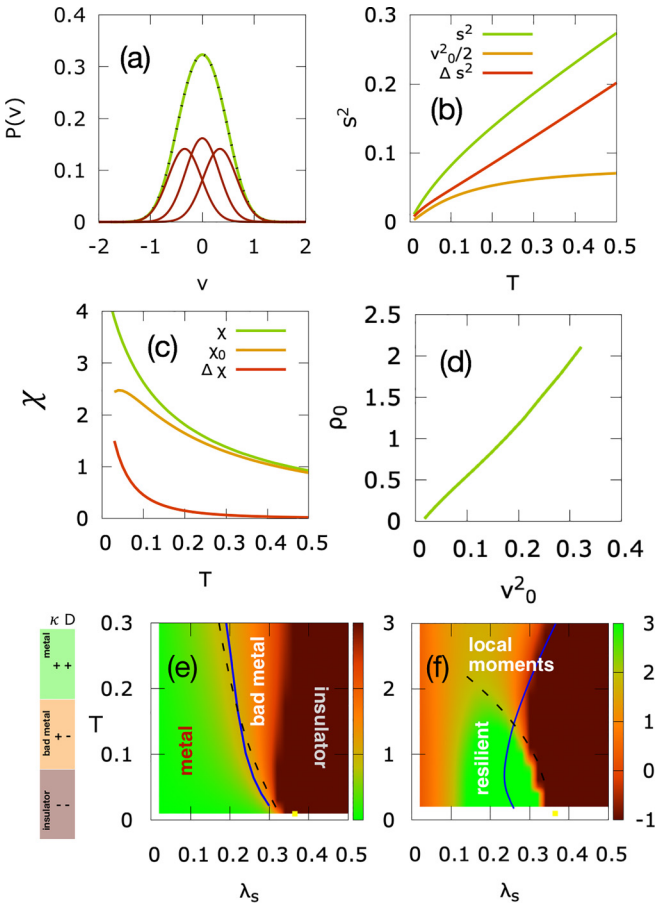


FIG. 2. (a) Symmetrized distributions  $P(v)$  of the SU(2) bosonic variable for  $T = 0.25$  and  $\lambda_s = 0.20$ , decomposed into the singly occupied, spin up (right Gaussian), spin down (left) and empty or doubly occupied sites (center). (b) Mean square fluctuation  $s^2 = \langle v^2 \rangle / 3$  as a function of temperature for  $\lambda_s = 0.20$  (green), compared with the residual term  $v_0^2$  (yellow) and the fluctuations  $\Delta s^2$  (red) extracted from the multicomponent fits of  $P(v)$ . (c) Local spin susceptibility (green) compared with its analogous decomposition into  $\chi_0$  (yellow) and  $\Delta\chi$  (red). (d) Residual resistivity  $\rho_0$  showing almost perfect correlation with the magnitude of the local moments  $v_0^2$  obtained at high temperature. (e) Map of the resistivity and (f) of the slope  $B$  in the  $(\lambda_s, T)$  plane. In (e) the black dashed curve is the MIR limit  $\rho = \rho_{\text{MIR}}$ , the blue curve locates the existence of a well formed pseudogap in the spectrum (see Appendix F), and the yellow square is the location of the MIT (estimated at  $T = 0.01$ ). The left legend indicates the magnitude of the charge compressibility  $\kappa$  and diffusivity  $\mathcal{D}$  entering the Nernst-Einstein relation [ $+$  ( $-$ ) stands for values  $>1$  ( $<1$ ); see Appendix D]. In (f) the black dashed curve locates the formation of local moments, and the blue curve is the point where the boson distribution becomes bimodal.

of scattering from fluctuating local moments. Figure 2(a) shows a typical radial distribution of the bosonic spin variable  $v$ , in the high-temperature metallic regime at moderate  $\lambda_s = 0.2$  ( $U/D = 1.2$ ). While at first sight the distribution seems Gaussian as predicted by perturbation theory, closer inspection reveals a hidden internal structure. The distribution obtained numerically can be perfectly described as the sum of three Gaussians of center  $\pm v_0, 0$  and variance  $\Delta s$ , originating respectively from singly occupied and empty or

doubly occupied sites;  $v_0$  and  $\Delta s$  represent the average magnitude and the magnitude fluctuations of the corresponding magnetic moments (see Appendix E).

Figure 2(b) shows the calculated mean square fluctuation  $s^2 = \langle v^2 \rangle / 3$  that determines the total scattering strength. The result can be written as  $s^2 = \Delta s^2 + v_0^2/2$ , separating explicitly the contributions to scattering originating from magnitude and angular fluctuations (because the orientation of the moments is undetermined, the impact of angular fluctuations is proportional to the magnitude  $v_0$ ). The magnitude fluctuations closely follow the classical thermal dependence,  $\Delta s^2 \simeq 2\lambda_s T$ . More interestingly to us,  $v_0^2/2$  reveals the angular fluctuations kicking in due to the emergence of local moments in the correlated metal phase. The residual resistivity of electrons scattered by randomly oriented moments is readily evaluated to  $\rho_0 \propto v_0^2$ . As reported in Fig. 2(d), this behavior is fully compatible with the resistivity data of Fig. 1, showing that the zero-temperature intercept of the resistivity is caused by the angular fluctuations of the local moments.

Finally, from the knowledge of  $s^2$  we can derive the *local* spin susceptibility [29] shown in Fig. 2(c). The latter appears to be dominated by the preformed moments, exhibiting the familiar Curie form  $\chi_s \sim 1/T$  even at high temperatures where the thermal fluctuation part  $\Delta s$  is much larger than the mean  $v_0$ .

#### IV. TRANSPORT PHASE DIAGRAM

The relation between the statistical properties of the spin variable and the transport mechanism is illustrated in Figs. 2(d) and 2(e), showing maps of the resistivity and its derivative in the  $(\lambda_s, T)$  plane. Figure 2(e) shows a progressive evolution of the resistivity as a function of the interaction strength  $\lambda_s$ , with values steadily increasing from the metal (left) to the Mott insulator (right). Bad metal behavior occurs in the intermediate coupling regime, where the resistivity rises above the Mott-Ioffe-Regel (MIR) limit (blue line). The bad metal regime defined by this condition is seen to coincide with the region where the momentum-integrated spectral density  $A(\omega) = -\text{Im} G(\omega)/\pi$  shows a well-formed pseudogap [21] [dashed line,  $A(0)$  equal to half of its maximum value; see Appendix A].

Figure 2(f) shows a map of the slope  $B$  in the same parameter range. Confirming the insights gained in the preceding sections, we see large variations of the slope upon varying  $\lambda_s$  at low  $T$ . At high  $T$ , however, the slope is essentially constant in a very broad region of parameters, that we associate with the fluctuating local moments phase. This is delimited by the dashed line, defined as the temperature at which the amplitude  $v_0$  of the local moments stabilizes above 80% of its high- $T$  saturation value; the color map shows that it coincides with the end of the resilient quasiparticle regime and the onset of strange metal transport, where the resistivity is  $T$  linear with almost universal slope. Also shown is the line beyond which the boson distribution becomes bimodal (blue); this coincides with the change of sign of the resistivity slope at high temperature and merges into a polaronic transition at  $T = 0$  (this is a precursor of the  $T = 0.0$  MIT, similar to the case of scalar coupling to the charge; see Appendix E and [20,30]).



## V. ORIGIN OF STRANGE METAL TRANSPORT

We now show that the character of the charge transport mechanism in the high-temperature regimes presented here is markedly non-Drude: the resistivity is *not* proportional to the scattering rate and it cannot be ascribed to (even ill-defined) quasiparticle carriers. To this aim we make a drastic simplification and rewrite the Kubo formula (4) by neglecting the band dispersion altogether. This corresponds to replacing the spectral function with its local (momentum integrated) equivalent  $A(\omega)$ , leading to  $\sigma_{\text{inc}} = 2\pi\tilde{\sigma} \int d\epsilon \Phi(\epsilon) \int d\omega [A(\omega)]^2 (-df/d\omega)$ , with  $\int d\epsilon \Phi(\epsilon) = D^2/4$  for the semicircular DOS (see Appendix C). The incoherent resistivity obtained through this formula accurately describes the numerical data up to a constant that is readily determined from the noninteracting limit by enforcing  $\rho(T=0) = 0$  (Fig. 1, dashed). Notably, the agreement extends down to the resilient quasiparticle regime, where it reproduces the correct  $\lambda_s^2$  dependence of the slope [standard weak-coupling approaches instead break down; see Fig. 1(b) and discussion].

With this paradigm shift at hand we can better understand the origin of the almost universal slope observed in the strange metal regime. In contrast to the low- $T$  limit, where the conductivity is determined by the value of the spectral function at the Fermi level, at high  $T$  excitations throughout the entire electronic spectrum are involved in the transport process. The leading  $T$  dependence of the resistivity can be understood by taking the high-temperature limit of the Fermi function,  $-df/d\omega \rightarrow 1/4T$ , showing that, as long as the temperature is comparable or larger than the range of variation of the spectral function  $A(\omega)$ , the resistivity is linear in  $T$  with an almost universal slope of order 1,  $B = d(\rho/\rho_{\text{MIR}})/dT \simeq (16/3\pi^2)/I$  being controlled by the global integral  $I = \int d\omega [A(\omega)]^2$ , a quantity that depends only weakly on model parameters. Indeed, magnetic fluctuations affect the integral via a mild increase of the effective bandwidth,  $D^* > D$  [31] resulting in  $B \simeq D^*/D = 1 + O(\lambda_s T/D)$ . Figure 1(b) shows that the slope for incoherent transport stabilizes around  $B \approx 1.5$ –2 in the whole range where strange metal is observed. Because it follows from global properties of the electronic spectrum, this result is largely independent on dimensionality, it does not rely on the existence of a quantum critical point, and it is robust upon combining different sources of scattering, as we show next.

## VI. INTERPLAY WITH DISORDER AND PHONON SCATTERING

Figure 3(a) shows that the addition of even a modest amount of scalar disorder (here taken to be Gaussian distribution of site energies with standard deviation  $\sigma$ ) tends to erase the clear distinction between the resilient quasiparticle regime and the strange metal found in the absence of disorder. The resistivity curves at different values of  $\sigma$  mainly differ by the value of their zero temperature intercept, but otherwise have a common slope that is largely unaffected by disorder. This agrees with what is observed in transport experiments of correlated systems under irradiation [9,32,33].

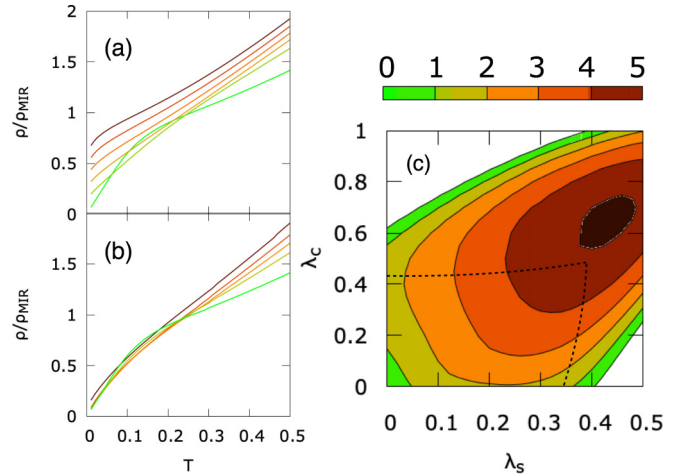


FIG. 3. (a) Resistivity vs  $T$  for  $\lambda_s = 0.2$  and different amounts of Gaussian scalar disorder with mean square fluctuation  $\sigma^2 = 0.0 \rightarrow 0.5$  and (b) different values of the charge coupling  $\lambda_c = 0.00 \rightarrow 0.32$  (from green to brown). (c) Map of the slope at  $T = 0.5$  in the  $(\lambda_s, \lambda_c)$  plane; the black dashed line marks the MIT (estimated at  $T = 0.01$ ).

Figure 3(b) shows the resistivity calculated in the presence of an added *scalar* electron-boson coupling,  $\lambda_c = g_0^2/2kD$ . Such interaction in the charge sector competes with the electronic correlations, shifting the Mott transition to higher values of  $\lambda_s$ . This competition is illustrated in the phase diagram of Fig. 3(c), showing the locus of the MIT (dashed line) superimposed on the map of the high-temperature slope  $B$ .

## VII. CONCLUDING REMARKS

The incoherent scattering of electrons from fluctuating local moments is able to explain the high-temperature strange metal behavior often observed in correlated electron systems. At odds with the normal Fermi liquid picture, in this regime the electrical conduction involves all states in the electronic spectrum instead of being governed by quasiparticle states near the Fermi energy alone: this leads to high- $T$ -linear resistivities with almost universal slopes that are insensitive to microscopic model details and qualitatively compatible with Planckian theoretical estimates. The microscopic mechanism unveiled here relies entirely on local physics, and is therefore alternative to existing hydrodynamic approaches to strange metals [34,35]. We also identify the primary sources of scattering to bosonic thermal excitations coupled spin degree of freedom, whereas scattering with overdamped bosonic excitation was recently put forward [36] to explain resonant x-ray scattering experiments in cuprates.

Interestingly, the “no quasiparticle” viewpoint helps in understanding the origin of the mysterious compensation of the  $T$  dependences of diffusivity and compressibility observed in previous numerical studies of correlated metals, with these two quantities seemingly conspiring to provide an overall  $\rho \propto T$  behavior [11,27,37]: our results show that in the strange metal regime the resistivity itself is the relevant physical quantity embodying the linear temperature dependence.

Remarkably, the inclusion of other sources of disorder in addition to the considered fluctuating local moments stabilizes

strange metal behavior down to the lowest temperatures, as observed in a variety of correlated metals. While identifying the precise nature of this missing randomness goes beyond the scope of this work, the generality of the experimental observations would hint at an intrinsic origin. Nearly frozen, self-generated disorder brought about by frustrated (magnetic [38] or charge [37,39–41]) interactions and surviving down to the lowest temperatures could be a plausible candidate.

Finally, due to its modest computational cost the approach introduced here could serve as a meaningful starting point for realistic simulations of correlated materials, as well as in all these systems (interfaces, mesoscopic devices and disordered systems) where the effects of spatial inhomogeneity beyond single- and few-site clusters are crucial.

### ACKNOWLEDGMENTS

This work has been funded by the European Union - NextGenerationEU under the Italian Ministry of University and Research (MUR) National Innovation Ecosystem Grant No. ECS00000041 - VITALITY - CUP E13C22001060006.

### APPENDIX A: DERIVATION OF THE DMFT RECURSION SCHEME

The action shown in Eqs. (1)–(3) can be derived by the following Hamiltonian within single site DMFT [23]:

$$H = -t \sum_{(i,j),\sigma} c_{i,\sigma}^\dagger c_{j,\sigma} + \sum_{i,\sigma,\rho} \sum_{\nu=0}^3 g_\nu c_{i,\sigma}^\dagger \sigma_{\sigma,\rho}^\nu c_{j,\rho} X_i^\nu + \frac{1}{2} \sum_\nu k_\nu (X_i^\nu)^2, \quad (\text{A1})$$

where  $c_{i,\sigma}^\dagger$  are creation operators of electrons at site  $i$  and spin-component  $\sigma$ ,  $\sigma^\nu$  are the Pauli matrices with  $\nu = 0, 3$  ( $\sigma^0 = 1$ ), and  $X_i^\nu$  are the classical boson displacement operators. Electrons can hop with hopping integral  $t$  and interact with the classical bosons through their charge ( $\nu = 0$ ) and spin ( $\nu > 0$ ).

The impurity propagator can be derived by averaging the matrix

$$\hat{G}(\omega) = \frac{1}{G_0^{-1}(\omega) - \sum_{\nu=0}^3 g_\nu \sigma_{\sigma,\rho}^\nu X^\nu} \quad (\text{A2})$$

over the classical phonon bath.  $G_0$  is propagator associated to the Weiss field resulting from the integration of the lattice electrons [23], that we take to be independent on spin indices  $\sigma$  since we do not consider symmetry broken phases. The classical distribution functions for the bosons can be derived by integrating out the Gaussian electronic degree of freedom using the action equations (1)–(3) of the main text:

$$P(X^\nu) \propto \exp(-S_b) \Pi_n \det \left( G_0^{-1}(i\omega_n) \mathbf{1} - \sum_{\nu=0}^3 g_\nu \sigma^\nu X^\nu \right). \quad (\text{A3})$$

In the nonordered phase the impurity propagator obtained by averaging the matrix (A2) with probability distribution (A3)

is spin independent and equal to

$$G(\omega) = \left\langle \frac{G_0^{-1}(\omega) + g_0 X^0 + \vec{v}(X^\nu) \cdot \boldsymbol{\sigma}}{(G_0^{-1}(\omega) - g_0 X^0)^2 - |\vec{v}(X^\nu)|^2} \right\rangle, \quad (\text{A4})$$

where  $\vec{v}$  is a three-dimensional vector of components  $v^\nu = g_\nu X^\nu$  ( $\nu = 1, 3$ ). The average over the classical boson variables restores translational invariance. The self-consistency condition is obtained by equating the impurity propagator with the local lattice propagator. Taking into account that in the paramagnetic case the self-energy is spin independent, we can write  $G(\omega) = G_0^{-1}(\omega) - \Sigma(\omega)$  and

$$G(\omega) = \int d\epsilon N(\epsilon) \frac{1}{\omega + \mu - \epsilon - \Sigma(\omega)}, \quad (\text{A5})$$

where  $N(\epsilon)$  is the noninteracting density of states (DOS) and  $\mu$  the chemical potential.

In the DMFT calculation of the optical conductivity via the Kubo formula, vertex corrections are absent. In the paramagnetic charge disordered case we obtain the usual expression [23]

$$\text{Re } \sigma(\omega) = 2\bar{\sigma} \pi \int d\epsilon \int d\nu \Phi(\epsilon) A(\epsilon, \nu) A(\epsilon, \omega + \nu) \times \frac{f(\nu) - f(\omega + \nu)}{\omega}, \quad (\text{A6})$$

where  $A(\epsilon, \nu) = -\text{Im} \frac{1}{\pi} [\omega + \mu - \epsilon - \Sigma(\omega)]^{-1}$  is the spectral function,  $\Phi(\epsilon) = \sum_k |v_k|^2 \delta(\epsilon - \epsilon_k)$  is the transport function in a given direction [ $v_k = \partial \epsilon(k)/\partial k$ ],  $f(\nu)$  is the Fermi function, and  $\bar{\sigma} = e^2 a^2 / \Omega \hbar$  is the unit of conductivity with  $a$  the lattice spacing in the chosen direction and  $\Omega$  the volume of the unit cell. The DC conductivity is readily obtained as the zero frequency limit of the expression above,

$$\sigma(T) = 2\bar{\sigma} \pi \int d\epsilon \Phi(\epsilon) \int d\omega A^2(\omega, \epsilon) \left( -\frac{df}{d\omega} \right). \quad (\text{A7})$$

We consider an isotropic spin coupling preserving SU(2) symmetry ( $g_\nu \equiv g_s$  for  $\nu = 1, 3$ ) and half filling ( $\mu = 0$ ). In this case the distribution of the bosonic fields depends only on two variables:  $X^0$ , coupled to the charge, and the modulus of the boson displacement coupled to the spin,  $r = \sqrt{\sum_{\nu=1}^3 (X^\nu)^2}$ . Integrating out the electrons gives

$$P(X^0, r) \propto \exp \left( -\frac{\beta}{2} [k_0 (X^0)^2 + k_s r^2] \right) \times \Pi_{n>0} |G_0^{-1}(i\omega_n) - g_0 X^0 - g_s r|^2 \times |G_0^{-1}(i\omega_n) - g_0 X^0 + g_s r|^2, \quad (\text{A8})$$

where we have used the fact that  $G_0^{-1}(-i\omega_n) = [G_0^{-1}(i\omega_n)]^*$ .

This probability distribution is even in the variable  $X^0$  and depends on the variables coupled to the spin only through the modulus  $r$ . The averages appearing in Eq. (A4) therefore simplify to

$$G(\omega) = \left\langle \frac{G_0^{-1}(\omega)}{(G_0^{-1}(\omega) - g_0 X^0)^2 - g_s^2 r^2} \right\rangle, \quad (\text{A9})$$

where we have defined the average appearing in Eq. (A9) as

$$\langle(\dots)\rangle = 4\pi \int dX_0 \int dr r^2(\dots).$$

Two dimensionless coupling constants can be defined in this problem: the charge coupling  $\lambda_c = g_0^2/2k_0D$  and the spin coupling  $\lambda_s = g_s^2/2k_sD$ . Accordingly we introduce two energy variables  $u = g_0X^0$  and  $v = g_s r$ . Since from Eq. (A8)  $P(X^0, r) = P(X^0, -r)$ , we can redefine the probability distribution of  $v$  by extending it to both positive and negative values of  $v$  as

$$\begin{aligned} P(u, v) \propto \exp \left[ - \left( \frac{u^2}{4\lambda_c DT} + \frac{v^2}{4\lambda_s DT} \right) \right] \\ \times \Pi_{n>0} |G_0^{-1}(i\omega_n) - u - v|^2 \\ \times |G_0^{-1}(i\omega_n) - u + v|^2. \end{aligned} \quad (\text{A10})$$

Equation (A9) can now be rewritten in a more compact form as

$$G(\omega) = \left\langle \frac{1}{G_0^{-1}(\omega) - u - v} \right\rangle, \quad (\text{A11})$$

where the average is taken on the two-variable distribution  $(4\pi v^2)P(u, v)$ .

All calculations presented here are performed on a Bethe lattice with an infinite coordination number  $z \rightarrow \infty$  and half bandwidth  $D = \sqrt{z}t$ , taking  $D$  as the energy unit. The corresponding DOS and transport function appearing in Eqs. (A5) and (A6) read [42]

$$N(\epsilon) = \frac{2}{\pi D^2} \sqrt{D^2 - \epsilon^2}, \quad (\text{A12})$$

$$\Phi(\epsilon) = \frac{2}{3\pi D^2} (D^2 - \epsilon^2)^{3/2}, \quad (\text{A13})$$

with  $\int \Phi(\epsilon) d\epsilon = D^2/4$ . On the Bethe lattice  $G_0^{-1}(i\omega_n) = i\omega_n - \frac{D^2}{4} G(i\omega_n)$  is known analytically. Equations (A11) and (A8) form a set of closed equations for the local Green's function  $G(i\omega_n)$  that can be easily solved numerically by recursion.

### APPENDIX B: RESISTIVITY AT THE MIR LIMIT

By replacing  $-df/d\omega = \delta(\omega - E_F)$  as appropriate at low temperatures and taking the weak scattering limit  $\Gamma(E_F) = -2 \text{Im} \Sigma(E_F) \ll D$ , one obtains  $\sigma = 2\bar{\sigma} \Phi(E_F)/\Gamma(E_F)$ ; cf. [25]. Observing that  $2\bar{\sigma} \Phi(E_F) = ne^2/m$  for a parabolic dispersion in any dimensions recovers the Drude formula,  $\sigma = ne^2\tau/m$ , with  $\tau = 1/\Gamma$ .

Defining the Mott-Ioffe-Regel limit through the condition  $k_F \ell = 1$  corresponds to  $\Gamma = 2E_F$ , yielding

$$\sigma_{\text{MIR}} = \bar{\sigma} \Phi(E_F)/E_F \quad (\text{B1})$$

on the parabolic band, with  $\bar{\sigma} = e^2 a^2 / \hbar \Omega$ . This allows us to define  $\rho_{\text{MIR}} = 1/\sigma_{\text{MIR}} = (3\pi/2)/\bar{\sigma}$  for the chosen semicircular density of states, if we set  $E_F = D$  at half filling. In these units, the low-temperature limit of Eq. (A7) acquires the simple expression

$$\rho/\rho_{\text{MIR}} = \Gamma/2D. \quad (\text{B2})$$

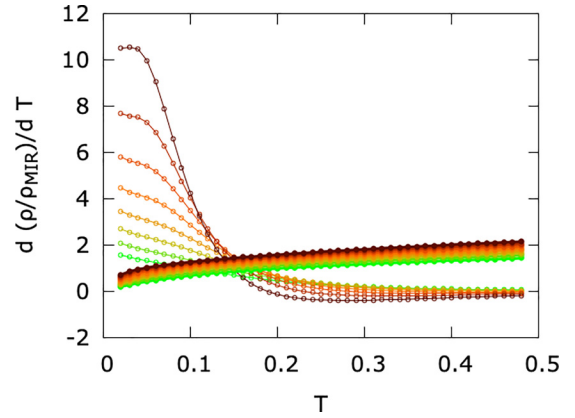


FIG. 4. The TCRs of  $\rho_\infty$  (closed symbols) and  $\Delta\rho$  (open symbols) compared. The coupling ranges from  $\lambda_s = 0.10$  (green) to  $\lambda_s = 0.24$  (dark brown).

### APPENDIX C: THE INCOHERENT SCATTERING REGIME

In the incoherent scattering regime we start with the Kubo formula and implement the following high-temperature decoupling in the derivative of the Fermi function appearing in Eq. (4):

$$\left( -\frac{df}{d\omega} \right) = \frac{1}{4T} [1 - \tanh^2(\omega/2T)]. \quad (\text{C1})$$

Correspondingly the conductivity can be written as  $\sigma = \sigma_\infty - \Delta\sigma$ , where

$$\sigma_\infty(T) = 2\bar{\sigma} \pi \frac{1}{4T} \int d\epsilon \Phi(\epsilon) \int d\omega A^2(\epsilon, \omega). \quad (\text{C2})$$

By defining  $\rho_\infty = 1/\sigma_\infty$  we can decouple the resistivity in a similar fashion as  $\rho = \rho_\infty + \Delta\rho$ . Figure 4 shows that at high temperatures the variation with temperature of  $\Delta\rho$  is negligible with respect to (w.r.t.) that of  $\rho_\infty$ . We now evaluate the temperature coefficient of the resistivity (TCR,  $B = d\rho/dT$ ) by considering the temperature variation of  $\rho_\infty$ . To provide an analytical estimate we take the incoherent approximation for the conductivity bubble,

$$\int d\epsilon \Phi(\epsilon) \int d\omega A^2(\epsilon, \omega) \simeq \frac{D^2}{4} \int d\omega A^2(\omega), \quad (\text{C3})$$

where  $A(\omega)$  is the (momentum-integrated) spectral density. Within this approximation we obtain

$$d\rho_\infty/dT = \frac{8}{\pi \bar{\sigma} D^2 \int d\omega A^2(\omega)} \quad (\text{C4})$$

Using Eq. (B1) we can write more generally

$$\frac{d\rho_\infty/\rho_{\text{MIR}}}{d(T/D)} = C(T) \quad (\text{C5})$$

with  $C(T)$  a dimensionless coefficient given by

$$C(T) = \frac{2\Phi(0)/\int \Phi(\epsilon) d\epsilon}{\pi \int d\omega A^2(\omega)} \quad (\text{C6})$$

for any lattice model and dimensionality.

The weak temperature dependence of this factor comes from the temperature dependence of the spectral function, due

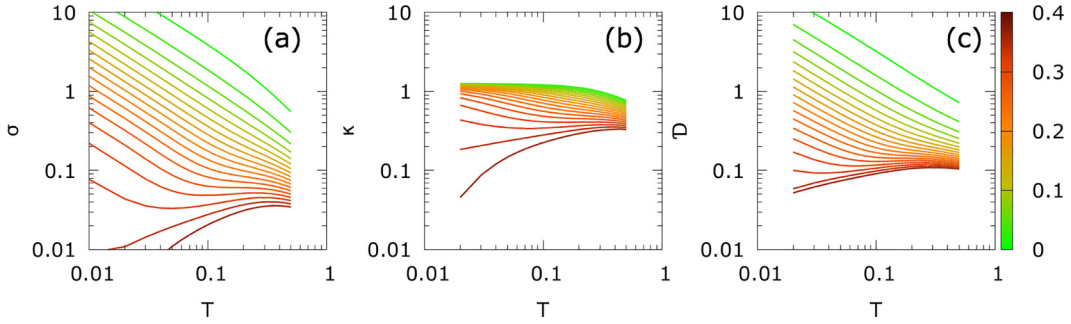


FIG. 5. (a) Conductivity, (b) compressibility, and (c) diffusivity as functions of temperature for  $\lambda_c = 0.0$  and  $\lambda_s$  spanning from 0.0 to 0.4 (from green to red).

to interactions with the thermal bosons. In the classical limit the coupling with the bosons provides an effective disorder potential that broadens the original DOS [31]. Since  $A(\omega)$  is normalized to 1, the integral appearing in Eq. (C6) is of the order of  $1/D^*(T)$ , where  $D^* \simeq D\sqrt{1 + 8\lambda_s T/D}$  as can be estimated in the Gaussian limit [31], therefore providing only a moderate preasymptotic temperature dependence. The order of magnitude of  $C$  can therefore be estimated using free-electron DOS: on the Bethe lattice  $\Phi(0) = 2D/3\pi$ ,  $\int \Phi(\epsilon)d\epsilon = D^2/4$ , and the integral in Eq. (C6) is  $16/3\pi^2 D$ , leading to  $C = 1$ .

The fact that the function  $\Phi$ , that embodies the specific properties of the lattice, appears both in the numerator and in the denominator of Eq. (C6) makes this estimate quite robust. For example, repeating the same calculation for a boxlike DOS mimicking the two-dimensional lattice yields  $C = 0.995$ .

#### APPENDIX D: NERNST-EINSTEIN ANALYSIS

The Nerst-Einstein relation

$$\sigma = e^2 \kappa \mathcal{D} \quad (\text{D1})$$

relates the conductivity  $\sigma$  to the compressibility  $\kappa$  and the diffusivity  $\mathcal{D}$ . In Eq. (D1),  $\sigma$  is known from the Kubo formula [Eq. (4), main text] whereas the compressibility can be derived by differentiating the particle number

$$n = \int d\nu f(\nu)A(\nu) \quad (\text{D2})$$

w.r.t.  $\mu$ . The diffusivity is obtained from these two quantities, via Eq. (D1).

The temperature dependence of the quantities  $\sigma$ ,  $\kappa$  and  $\mathcal{D}$  is shown in Fig. 5 for  $\lambda_c = 0.0$ , enabling a qualitative understanding of the different transport regimes. At weak coupling both diffusivity and compressibility are large and the temperature dependence of the conductivity is driven by the diffusivity [11,13]. At strong coupling both the compressibility and the diffusivity are suppressed, leading to low-temperature insulating behavior.

Interestingly, the strange metallic regime at high temperature and moderate  $\lambda_s \simeq 0.2-0.3$  is characterized by a sizable compressibility in comparison to the insulating phase, together with a suppressed diffusivity. The + and - signs in the legend of Fig. 2(e) of the main text indicate the qualitative amplitude of the components  $\kappa$  and  $\mathcal{D}$  in the different regimes

of the phase diagram; the symbols + and - indicate sizable and suppressed values respectively.

We note that in the strange metallic regime the  $1/T$  behavior of the conductivity cannot be ascribed individually to  $\kappa$  or  $\mathcal{D}$ . Here the conductivity itself is the key quantity that carries the strange metal properties ( $\rho \sim T$ ), while  $\kappa$  and  $\mathcal{D}$  show no obvious power law behavior.

Figure 6 reports the  $\lambda_s$  dependence of  $\sigma$ ,  $\kappa$ , and  $\mathcal{D}$  at a fixed temperature  $T = 0.2$ . At weak coupling the compressibility is close to 1; the variation of  $\sigma$  is dominantly driven by a reduction of the diffusivity with  $\lambda_s$ . Upon entering the strange metallic regime the reduction of conductivity results from a concomitant, yet weaker, decrease of both  $\kappa$  and  $\mathcal{D}$ . Importantly, the diffusivity does not seem to saturate to any lower bound, in contradiction with recent proposals based on hydrodynamics [43].

#### APPENDIX E: THE ATOMIC LIMIT, BOSON DISTRIBUTION, AND LOCAL SPIN SUSCEPTIBILITY

In the atomic limit  $D \rightarrow 0$  we can rewrite the Hamiltonian as

$$H = H_b(X_0, r) + (g_0 X_0 - \mu)n + g\vec{\sigma} \cdot \vec{X} \quad (\text{E1})$$

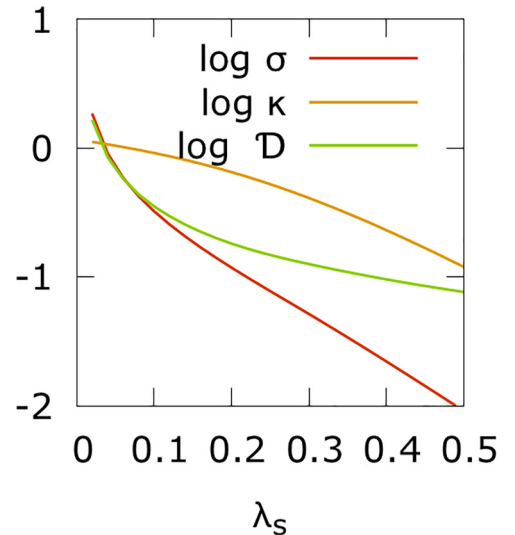


FIG. 6. Logarithms of conductivity, compressibility, and diffusivity as functions of  $\lambda_s$  at  $T = 0.2$ . All quantities are expressed in units where  $a = D = e = 1$



where the boson part of the Hamiltonian is  $H_b(X_0, r) = \frac{1}{2}k_0X_0^2 + \frac{1}{2}kr^2$ ,  $r^2 = \sum_{v=1}^3 X_v^2$ , and  $n = n_\uparrow + n_\downarrow$ . The half-filling condition is  $\mu = \mu_0 = -g_0/k_0$ . Upon shifting the chemical potential as  $\mu' = \mu + g_0/k_0$  and the displacement coupled to the charge  $X'_0 = X_0 + g_0/k_0$ , the four electronic states for any given value of classical displacements  $X_v$  have the following energies:

$$|0\rangle : \Omega_0 = H_b(X'_0, r) - g_0X'_0, \quad (\text{E2})$$

$$|+\rangle : \Omega_{1,+} = H_b(X'_0, r) - \mu' + gr, \quad (\text{E3})$$

$$|-\rangle : \Omega_{1,-} = H_b(X'_0, r) - \mu' - gr, \quad (\text{E4})$$

$$|\uparrow, \downarrow\rangle : \Omega_2 = H_b(X'_0, r) - 2\mu' + g_0X'_0 \quad (\text{E5})$$

[here  $H_b(X'_0, r)$  is the Gaussian part rewritten in terms of the shifted  $X'_0$ ].

By introducing the variables  $u = g_0X'_0$  and  $v = gr$ , the partition function reads

$$Z = \int du dv 4\pi v^2 e^{-\beta H_b} (e^{\beta u} + 2 \cosh(\beta v) e^{\beta \mu'} + e^{\beta(2\mu' - u)}) \quad (\text{E6})$$

with  $H_b = u^2/4\lambda_c D + v^2/4\lambda_s D$ . We can now define a distribution function for the variables coupled to the spin ( $v$ ) and to the charge ( $u$ ), that we write at half filling for sake of simplicity:

$$4\pi v^2 P(u, v) = \frac{4\pi v^2}{Z} \exp\left(-\frac{\beta u^2}{4\lambda_c D} - \frac{\beta v^2}{4\lambda_s D}\right) \times [\cosh(\beta u) + \cosh(\beta v)]. \quad (\text{E7})$$

In the expression above, the Jacobian  $4\pi v^2$  accounts for the the SU(2) nature of the spin fluctuations, and  $v$  extends to the whole  $-\infty, \infty$  range. The  $\cosh \beta u$  term in Eq. (E7) is the contribution from empty and doubly occupied sites. When multiplied by the exponential prefactor it gives rise to two Gaussians in the variable  $u$  peaked around  $u_0 = \pm 2\lambda_c D$ . The term proportional to  $\cosh \beta v$  comes from the singly occupied sites and again gives rise to two Gaussians in the variable  $v$ , peaked around  $v_0 = \pm 2\lambda_s D$ . In the case of a pure spin coupling only three Gaussian contributions remain in the variable  $v$ : one peaked around  $v = 0$  coming from doubly occupied and empty sites, and two peaks at symmetric values of  $v = \pm v_0$  arising from singly occupied sites. The fitting procedure of Fig. 2(a) is based on this result.

When generalized to include both spin- and charge-coupled fields with displacements  $v_0, u_0$  and general variances  $\sigma_s^2, \sigma_c^2$  the distribution Eq. (E7) reads

$$4\pi v^2 P(u, v) = \frac{4\pi v^2}{Z} \exp\left(-\frac{u^2}{2\sigma_c^2} - \frac{v^2}{2\sigma_s^2}\right) \times \left[ \cosh\left(\frac{u_0 u}{\sigma_c^2}\right) + \cosh\left(\frac{v_0 v}{\sigma_s^2}\right) \right]. \quad (\text{E8})$$

In the case of pure spin coupling Eq. (E8) simplify to

$$4\pi v^2 P(v) = \frac{4\pi v^2}{Z} \exp\left(-\frac{v^2}{2\sigma_s^2}\right) \times \left[ 1 + \cosh\left(\frac{v_0 v}{\sigma_s^2}\right) \right], \quad (\text{E9})$$

which is the form from which the DMFT data were fitted in Fig. 2 of the main text. Using the distribution Eq. (E8) one can derive the following results:

$$\langle v^2 \rangle = 3\sigma_s^2 \frac{(x_0^4/3 + 2x_0^2 + 1)e^{\frac{x_0^2}{2}} + 1}{(x_0^2 + 1)e^{\frac{x_0^2}{2}} + 1}, \quad (\text{E10})$$

$$\langle u^2 \rangle = \sigma_c^2 \frac{(x_0^2 + 1)e^{\frac{x_0^2}{2}} + 1}{e^{\frac{x_0^2}{2}} + 1}, \quad (\text{E11})$$

valid respectively in the case of pure spin [Eq. (E10)] and in the case of pure charge [Eq. (E11)] couplings. In Eq. (E10)  $x_0 = v_0/\sigma_s$  and in Eq. (E11)  $x_0 = u_0/\sigma_c$ . In the limit  $x_0 \ll \sigma$  we obtain from Eq. (E10)  $s^2 \equiv \langle v^2 \rangle/3 = \sigma_s^2 + v_0^2/2$  for  $\lambda_c = 0$  as reported in the main text. For  $\lambda_s = 0$  we have instead  $\langle u^2 \rangle = \sigma_c^2 + u_0^2$ .

Using the general result derived in Ref. [29] we can relate the variance of the centroid distribution of Stratonovich-Hubbard bosons to the local spin (or charge) susceptibility. Using Eq. (9) of Ref. [29] we have

$$\chi^{\text{loc}} = \frac{1}{2\lambda_v D} \left( \frac{\langle \Delta^2 X_v \rangle}{\langle \Delta^2 X_v \rangle_0} - 1 \right), \quad (\text{E12})$$

where  $\chi^{\text{loc}}$  is the local susceptibility to an external field which couples to the charge ( $v = 0$ ) or to the spin ( $v = 1, 2, 3$ ),  $\lambda_v$  is the coupling (spin or charge), and  $\langle \Delta^2 X_v \rangle$  is the mean-square

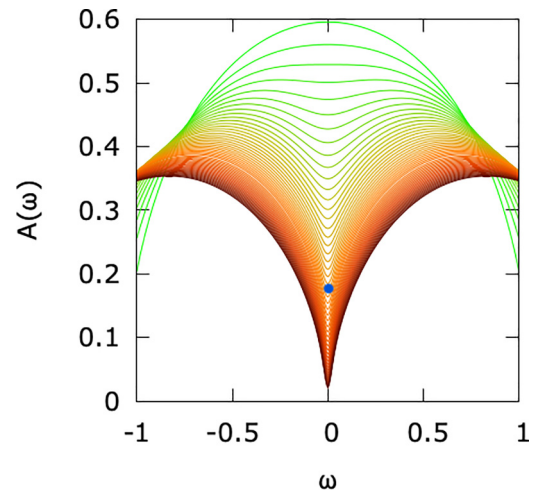


FIG. 7. Spectral function vs temperature at  $\lambda_s = 0.20$  and  $\lambda_c = 0.00$ ;  $T$  ranges from 0.02 to 0.50. The blue dot indicates the pseudo-gap value at  $T = 0.25$ .



displacement of the bosonic field whereas  $\langle \Delta^2 X_v \rangle_0$  is the same evaluated in the noninteracting system.

In the limit  $v_0^2 < \sigma_s^2$  [see Eqs. (E10) and (E12)] the local spin susceptibility can be decomposed into  $\chi^{\text{loc}} = \chi_0 + \Delta\chi$ , where

$$\chi_0 = \frac{1}{2\lambda_s D} \frac{v_0^2}{2\sigma_0^2} \quad (\text{E13})$$

is the term associated with the local moments and  $\sigma_0^2 = 2\lambda_s D T$ . The contribution associated with fluctuations reads

$$\Delta\chi = \frac{1}{2\lambda_s D} \left( \frac{\sigma_s^2}{\sigma_0^2} - 1 \right). \quad (\text{E14})$$

Notice that approaching the atomic limit, Eq. (E13), gives rise to the Curie  $1/T$  behavior for the local spin susceptibility.

## APPENDIX F: SPECTRAL FUNCTION AND MIT

Figure 7 illustrates the opening of a pseudogap in the spectral function for  $\lambda_s = 0.20$  as a function of temperature. The blue dot marks the pseudogap value at the temperature  $T = 0.25$  corresponding to the distribution  $P$  depicted in Fig. 2(a). While the radial distribution of the spin variable  $v$  does not show a well-defined peak, a pseudogap is formed in the spectral function as consequence of the SU(2) nature of the spin fluctuations, via the Jacobian  $4\pi v^2$  that effectively splits the distribution into two separate peaks. In the local moment regime a pseudogap forms gradually in the spectral function upon increasing  $\lambda_s$ , eventually leading to a genuine MIT at  $T = 0.0$  at a critical value of the spin coupling. The pseudogap also arises upon increasing  $T$ , without however inducing a MIT; at high temperatures the system behaves as a strange metal as described in the preceding sections and in the main text.

- 
- [1] J. Zaanen, Planckian dissipation, minimal viscosity and the transport in cuprate strange metals, *SciPost Phys.* **6**, 061 (2019).
- [2] S. A. Hartnoll and A. P. Mackenzie, Colloquium: Planckian dissipation in metals, *Rev. Mod. Phys.* **94**, 041002 (2022).
- [3] J. A. N., B. H. Sakai, R. S. Perry, and A. P. Mackenzie, Similarity of scattering rates in metals showing  $T$ -linear resistivity, *Science* **339**, 804 (2013).
- [4] A. Legros, S. Benhabib, W. Tabis, F. Laliberté, M. Dion, M. Lizaire, B. Vignolle, D. Vignolles, H. Raffy, Z. Z. Li, P. Auban-Senzier, N. Doiron-Leyraud, P. Fournier, D. Colson, L. Taillefer, and C. Proust, Universal  $T$ -linear resistivity and Planckian dissipation in overdoped cuprates, *Nat. Phys.* **15**, 142 (2019).
- [5] P. W. Phillips, N. E. Hussey, and P. Abbamonte, Stranger than metals, *Science* **377**, eabh4273 (2022).
- [6] H. Terletska, J. Vučičević, D. Tanasković, and V. Dobrosavljević, Quantum critical transport near the Mott transition, *Phys. Rev. Lett.* **107**, 026401 (2011).
- [7] J. Vučičević, J. Kokalj, R. Žitko, N. Wentzell, D. Tanasković, and J. Mravlje, Conductivity in the square lattice Hubbard model at high temperatures: Importance of vertex corrections, *Phys. Rev. Lett.* **123**, 036601 (2019).
- [8] Y. Suzuki, K. Wakamatsu, J. Ibuka, H. Oike, T. Fujii, K. Miyagawa, H. Taniguchi, and K. Kanoda, Mott-driven bec-bcs crossover in a doped spin liquid candidate  $\kappa$ -(BEDT-TTF)<sub>4</sub>Hg<sub>2.89</sub>Br<sub>8</sub>, *Phys. Rev. X* **12**, 011016 (2022).
- [9] M. Urai, T. Furukawa, Y. Seki, K. Miyagawa, T. Sasaki, H. Taniguchi, and K. Kanoda, Disorder unveils mott quantum criticality behind a first-order transition in the quasi-two-dimensional organic conductor  $\kappa$ -(ET)<sub>2</sub>Cu[N(CN)<sub>2</sub>]Cl, *Phys. Rev. B* **99**, 245139 (2019).
- [10] A. A. Patel, H. Guo, I. Esterlis, and S. Sachdev, Universal theory of strange metals from spatially random interactions, *Science* **381**, 790 (2023).
- [11] J. Kokalj, Bad-metallic behavior of doped Mott insulators, *Phys. Rev. B* **95**, 041110(R) (2017).
- [12] E. W. Huang, R. Sheppard, B. Moritz, and T. P. Devereaux, Strange metallicity in the doped Hubbard model, *Science* **366**, 987 (2019).
- [13] N. Pakhira and R. H. McKenzie, Absence of a quantum limit to charge diffusion in bad metals, *Phys. Rev. B* **91**, 075124 (2015).
- [14] E. Perepelitsky, A. Galatas, J. Mravlje, R. Žitko, E. Khatami, B. S. Shastry, and A. Georges, Transport and optical conductivity in the Hubbard model: A high-temperature expansion perspective, *Phys. Rev. B* **94**, 235115 (2016).
- [15] W. Wú, X. Wang, and A.-M. Tremblay, Non-Fermi liquid phase and linear-in-temperature scattering rate in overdoped two-dimensional Hubbard model, *Proc. Natl. Acad. Sci. USA* **119**, e2115819119 (2022).
- [16] P. Cha, A. A. Patel, E. Gull, and E.-A. Kim, Slope invariant  $T$ -linear resistivity from local self-energy, *Phys. Rev. Res.* **2**, 033434 (2020).
- [17] P. M. Lozano, G. D. Gu, Q. Li, and J. M. Tranquada, Strange-metal behavior in La<sub>2-x</sub>Sr<sub>x</sub>CuO<sub>4</sub> beyond the stripe-percolation transition, [arXiv:2307.13740](https://arxiv.org/abs/2307.13740).
- [18] E. Fradkin, *Field Theories of Condensed Matter Systems*, edited by D. Pines (Perseus, Cambridge, MA, 1991).
- [19] M. S. Scheurer, S. Chatterjee, W. Wu, M. Ferrero, A. Georges, and S. Sachdev, Topological order in the pseudogap metal, *Proc. Natl. Acad. Sci. USA* **115**, E3665 (2018).
- [20] A. J. Millis, R. Mueller, and B. I. Shraiman, Fermi-liquid-to-polaron crossover. I. General results, *Phys. Rev. B* **54**, 5389 (1996).
- [21] R. Tiwari and P. Majumdar, Spectroscopic signatures of the Mott transition on the anisotropic triangular lattice, *Europhys. Lett.* **108**, 27007 (2014).
- [22] S. Okamoto, A. Fuhrmann, A. Comanac, and A. J. Millis, Benchmarkings for a semiclassical impurity solver for dynamical-mean-field theory: Self-energies and magnetic transitions of the single-orbital Hubbard model, *Phys. Rev. B* **71**, 235113 (2005).
- [23] A. Georges, G. Kotliar, W. Krauth, and M. J. Rozenberg, Dynamical mean-field theory of strongly correlated fermion systems and the limit of infinite dimensions, *Rev. Mod. Phys.* **68**, 13 (1996).
- [24] T. Schäfer, F. Geles, D. Rost, G. Rohringer, E. Arrighoni, K. Held, N. Blümer, M. Aichhorn, and A. Toschi, Fate of the false

- Mott-Hubbard transition in two dimensions, *Phys. Rev. B* **91**, 125109 (2015).
- [25] X. Deng, J. Mravlje, R. Žitko, M. Ferrero, G. Kotliar, and A. Georges, How bad metals turn good: Spectroscopic signatures of resilient quasiparticles, *Phys. Rev. Lett.* **110**, 086401 (2013).
- [26] A. J. Millis, J. Hu, and S. DasSarma, Resistivity saturation revisited: Results from a dynamical mean field theory, *Phys. Rev. Lett.* **82**, 2354 (1999).
- [27] T. G. Kiely and E. J. Mueller, Transport in the two-dimensional Fermi-Hubbard model: Lessons from weak coupling, *Phys. Rev. B* **104**, 165143 (2021).
- [28] L. V. Delacrétaz, B. Goutéraux, S. A. Hartnoll, and A. Karlsson, Bad metals from fluctuating density waves, *SciPost Phys.* **3**, 025 (2017).
- [29] S. Ciuchi, G. Sangiovanni, and M. Capone, Pairing and polarization in electron-boson systems with retarded interactions via dynamical mean-field theory, *Phys. Rev. B* **73**, 245114 (2006).
- [30] M. Capone and S. Ciuchi, Polaron crossover and bipolaronic metal-insulator transition in the half-filled holstein model, *Phys. Rev. Lett.* **91**, 186405 (2003).
- [31] S. Fratini and S. Ciuchi, Spectral properties and isotope effect in strongly interacting systems: Mott-Hubbard insulator versus polaronic semiconductor, *Phys. Rev. B* **72**, 235107 (2005).
- [32] I. Vobornik, H. Berger, D. Pavuna, M. Onellion, G. Margaritondo, F. Rullier-Albenque, L. Forró, and M. Grioni, Spectroscopic signatures of defect-induced pair breaking in  $\text{Bi}_2\text{Sr}_2\text{CaCu}_2\text{O}_{8+x}$ , *Phys. Rev. Lett.* **82**, 3128 (1999).
- [33] F. Rullier-Albenque, H. Alloul, and R. Tourbot, Disorder and transport in cuprates: Weak localization and magnetic contributions, *Phys. Rev. Lett.* **87**, 157001 (2001).
- [34] A. Lucas and S. A. Hartnoll, Resistivity bound for hydrodynamic bad metals, *Proc. Natl. Acad. Sci. USA* **114**, 11344 (2017).
- [35] J. Vučičević, S. Predin, and M. Ferrero, Charge fluctuations, hydrodynamics, and transport in the square-lattice Hubbard model, *Phys. Rev. B* **107**, 155140 (2023).
- [36] G. Seibold, R. Arpaia, Y. Y. Peng, R. Fumagalli, L. Braicovich, C. Di Castro, M. Grilli, G. C. Ghiringhelli, and S. Caprara, Strange metal behaviour from charge density fluctuations in cuprates, *Commun. Phys.* **4**, 7 (2021).
- [37] C. H. Mousatov, I. Esterlis, and S. A. Hartnoll, Bad metallic transport in a modified Hubbard model, *Phys. Rev. Lett.* **122**, 186601 (2019).
- [38] M. Frachet, I. Vinograd, R. Zhou, S. Benhabib, S. Wu, H. Mayaffre, S. Krämer, S. K. Ramakrishna, A. P. Reyes, J. Debray, T. Kurosawa, N. Momono, M. Oda, S. Komiya, S. Ono, M. Horio, J. Chang, C. Proust, D. LeBoeuf, and M.-H. Julien, Hidden magnetism at the pseudogap critical point of a cuprate superconductor, *Nat. Phys.* **16**, 1064 (2020).
- [39] S. Mahmoudian, L. Rademaker, A. Ralko, S. Fratini, and V. Dobrosavljević, Glassy dynamics in geometrically frustrated Coulomb liquids without disorder, *Phys. Rev. Lett.* **115**, 025701 (2015).
- [40] K. Driscoll, A. Ralko, and S. Fratini, Pseudogap metal induced by long-range Coulomb interactions, *Phys. Rev. B* **103**, L201106 (2021).
- [41] S. Fratini and S. Ciuchi, Displaced Drude peak and bad metal from the interaction with slow fluctuations., *SciPost Phys.* **11**, 039 (2021).
- [42] A. Chattopadhyay, A. J. Millis, and S. Das Sarma, Optical spectral weights and the ferromagnetic transition temperature of colossal-magnetoresistance manganites: Relevance of double exchange to real materials, *Phys. Rev. B* **61**, 10738 (2000).
- [43] S. A. Hartnoll, Theory of universal incoherent metallic transport, *Nat. Phys.* **11**, 54 (2015).